LAWRENCE
LIVERMORE
NATIONAL
LABORATORY

LLNL-PROC-497653

# Precision X-Band Linac Technologies for Nuclear Photonics Gamma-Ray Sources

F. V. Hartemann, F. Albert, S. G. Anderson, A. J. Bayramian, R. R. Cross, C. A. Ebbers, D. J. Gibson, T. L. Houck, R. A. Marsh, M. J. Messerly, C. W. Siders, D. P. McNabb, C. P. J. Barty, C. E. Adolphsen, T. S. Chu, E. N. Jongewaard, S. G. Tantawi, A. E. Vlieks, F. Wang, J. W. Wang, T. O. Raubenheimer, D. Ighigeanu, M. Toma, D. Cutoiu

September 6, 2011

2nd International Particle Accelerator Conference
San Sebastian, Spain
September 4, 2011 through September 9, 2011

## Disclaimer

# PRECISION X-BAND LINAC TECHNOLOGIES FOR NUCLEAR PHOTONICS GAMMA-RAY SOURCES*

F.V. Hartemann, F. Albert, S. G. Anderson, A.J. Bayramian, R.R. Cross, C.A. Ebbers, D. J. Gibson, T.L. Houck, R.A. Marsh, M. J. Messerly, C.W. Siders, D.P. McNabb, C.P.J. Barty, LLNL, USA; C.E. Adolphsen, T.S. Chu, E.N. Jongewaard, S.G. Tantawi, A.E. Vlieks, F. Wang, J.W. Wang, T.O. Raubenheimer, SLAC, USA; D. Ighigeanu, M. Toma, INFLRP, Romania; D. Cutoiu, IFIN-HH, Romania

*Abstract*

Nuclear photonics is an emerging field of research requiring new tools, including high spectral brightness, tunable gamma-ray sources; high photon energy, ultrahigh-resolution crystal spectrometers; and novel detectors. This presentation focuses on the precision linac technology required for Compton scattering gamma-ray light sources, and on the optimization of the laser and electron beam pulse format to achieve unprecedented spectral brightness. Within this context, high-gradient X-band technology will be shown to offer optimal performance in a compact package, when used in conjunction with the appropriate pulse format, and photocathode illumination and interaction laser technologies.

## INTRODUCTION AND OVERVIEW

The nascent field of nuclear photonics is enabled by the recent maturation of new technologies, including high-gradient X-band electron acceleration, robust fiber laser systems, and hyper-dispersion CPA [1]. Recent work has been performed at LLNL to demonstrate isotope-specific detection of shielded materials via NRF using a tunable, quasi-monochromatic Compton scattering gamma-ray source operating between 0.2 MeV and 0.9 MeV photon energy. This technique is called Fluorescence Imaging in the Nuclear Domain with Energetic Radiation (or FINDER). This work has, among other things, demonstrated the detection of $^7$Li shielded by Pb, utilizing gamma rays generated by a linac-driven, laser-based Compton scattering gamma-ray source developed at LLNL [2-4]. Within this context, a new facility is currently under construction at LLNL, with the goal of generating tunable γ-rays in the 0.5-2.5 MeV photon energy range, at a repetition rate of 120 Hz, and with a peak brightness in the $10^{20}$ photons/(s x mm$^2$ x mrad$^2$ x 0.1% bw).

## COMPTON SCATTERING

This section is a brief summary of the main properties of Compton scattering. The incident electron and photon 4-momenta are given by $u_\mu=(\gamma,\mathbf{u})$ and $k_\mu=(k,\mathbf{k})$; the scattered photon 4-wavenumber is $q_\mu=(q,\mathbf{q})$, and the electron 4-velocity after the interaction satisfies energy-momentum conservation: $v_\mu=u_\mu+\lambda\!\!\!^{-}\left(nk_\mu-q_\mu\right)$, where $\lambda\!\!\!^{-}$ is the reduced Compton wavelength and $n$ is the harmonic (multi-photon) number. From these parameters, the incident and scattered light-cone variables can be computed [5], along with the Compton formula:

$$\frac{q}{k}=\frac{\gamma-u\cos\left(\varepsilon+\varphi\right)}{\gamma-u\cos\varepsilon+\left(1-\cos\varphi\right)\left\{\dfrac{\left\langle -A_\mu A^\mu\right\rangle}{2\left[\gamma-u\cos\left(\varepsilon+\varphi\right)\right]}+n\lambda\!\!\!^{-}k\right\}}.$$

Here, $\varepsilon$ is the angle between the electron initial velocity and the mean electron beam axis; $\varphi$ is the angle of incidence of the laser photon(s); $-A_\mu A^\mu$ corresponds to radiation pressure; finally, the result is given for on-axis radiation ($\theta=0$). The relativistic Doppler upshift, radiation pressure, and recoil are the main contributions to the scattered photon energy. This equation also shows that the frequency is very sensitive to both the electron beam and laser pulse phase spaces. Additional information can be derived from the Klein-Nishina differential scattering cross-section [6], 3D effects, and nonlinearities [7].

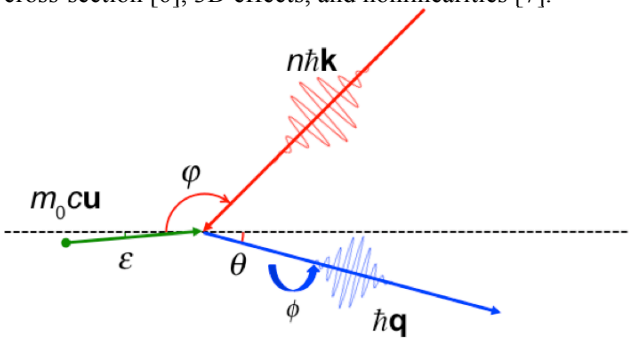


Figure 1: interaction geometry.

## X-BAND OPTIMUM

One of the key electron beam parameters leading to optimum brightness is the charge to normalized emittance squared ratio, $q/\varepsilon_n^2$. This quantity scales linearly with the cathode electric field in the injector [8]: $\dfrac{q}{\varepsilon_n^2}=\dfrac{m_0c^2E_0}{2k_BT}$.

* Work performed under the auspices of the U.S. Department of Energy by Lawrence Livermore National Laboratory under Contract DE-AC52-07NA27344.

In turn, the electric field increases with the rf frequency, as shown in Fig. 2, which summarizes experimentally achieved parameters at 3 different frequencies: 2.856 GHz, 8.547 GHz, and 11.424 GHz [9-11].

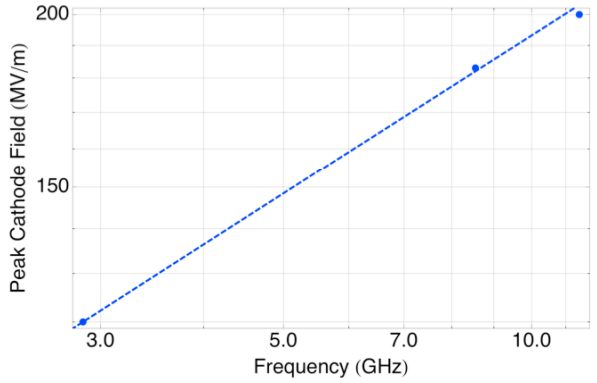


Figure 2: photocathode electric field vs. frequency.

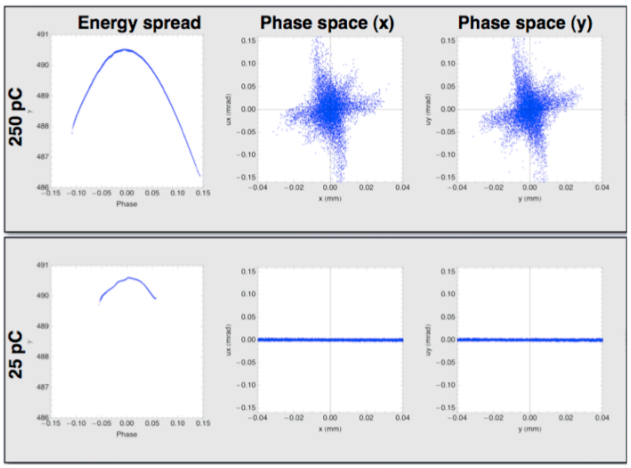


Figure 3: comparison between 25 and 250 pC bunches.

The dashed line corresponds to a $f^{0.38}$ fit. Full Parmela simulations confirm that $q/\varepsilon_n^2$ is invariant, as shown in Fig. 3, where the rf frequency is 11.424 GHz, the maximum photocathode electric field is 200 MV/m, and two different bunch charges are considered: 250 pC and 25 pC. In the first case, the normalized emittance is 0.35 mm.mrad, and the energy spread is 0.16%; in the low charge case, the normalized emittance is 0.1 mm.mrad, and the relative energy spread is 0.03%.

## X-BAND RF PHOTO-INJECTOR

The RF photoinjector is based on an earlier high gradient 7 MeV, 5.5-cell X-band RF photoinjector. Improvements specific to our application have been implemented and will be described in this paper. PARMELA simulations revealed that a longer first half-cell, as simulated with SUPERFISH resulted in a lower final emittance for the setup planned at LLNL. As a result a full redesign of the RF gun has been performed, using a longer first half-cell, lengthened from a 0.49 cell to a 0.59 cell. A schematic of the gun, low-energy beamline (LEB) and T53 is shown in Fig. 4.

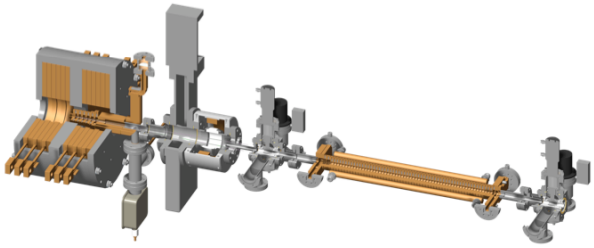

Figure 4: X-band RF gun, LEB, and T53 section.

Superior electron beam quality, with a normalized emittance of 0.35 mm.mrad at 250 pC charge, is ensured by the very high field applied to the photocathode: 200 MV/m, nominally. Full emittance compensation is implemented, with an optimum distance from the photocathode to the first accelerating section of 0.8 m.

The RF gun properties required for complete design are: field balanced across all cells, mode frequency of 11.424 GHz, and a coupling β of ~1.7. This new RF gun boasts an improved mode separation of >20 MHz, which decreases mode beating of the electric field on the cathode. The new RF gun also employs a racetrack coupler to reduce the RF quadrupole field experienced by the electron beam, and elliptically contoured irises to decrease the maximum surface electric field. These improvements were incorporated into the design of a modified RF gun for LLNL.

Complete 3D RF design for the photoinjector was accomplished using HFSS. Each modification affects the three design criteria: field balance is primarily a function of relative cell radii; coupling is primarily a function of the coupler cell radius and coupling aperture; the frequency is primarily changed by scaling all cell radii. Each adjustment changes the primary goal being modified, but also affects the other two. Final design is achieved by successive iteration, until all parameters are simultaneously met. The final field balance is quite excellent, and the final coupling was achieved at 11.424 GHz, with a β of ~1.7.

Final modification of the design is necessary to converge on a set of dimensions for engineering drawings and actual OFHC Cu fabrication. Machining will be done at 20ºC, while operation is planned for 45ºC. Scaling of the design dimensions was calculated and simulated. Design numbers were then truncated to acceptable fabrication tolerances, which required readjustment of the drawing numbers to conform with optimal field balance, coupling, and frequency at the operating temperature of 45ºC. Engineering drawings have been completed, and fabrication is planned in the near future.

## 0.5 GW X-BAND RF SYSTEM

The high power RF system is to provide adequate RF power to the accelerator to achieve the end-point electron energy. The accelerator consists of a X-band photo-gun and six sections of traveling wave accelerating structure,

the T53VG3. The X-band photo-gun is a modified version of the 5.49 cells RF gun tested at SLAC in 2002. The RF budget for the gun is 20 MW and the fill time of the structure is 65 ns. The T53VG3 type travelling wave structure was extensively tested for high gradient operation and has operated at high gradient with low breakdown rates. The T-series structures are essentially the low group velocity (downstream) portion of the original 1.8 m structures. This structure can be operated with acceptable trip rate at gradients up to 90 MV/m. The fill time of this structure is 74.3 ns and an RF power of 70 MW is budgeted for each section.

The high power RF source is a X-band klystron (XL-4), which was developed by SLAC in the mid 90's for the high power testing of the X-band structures. The XL-4 is a solenoid focused klystron which requires a 0.47 Tesla solenoid. The high voltage pulse required by the klystron is provided by a state of the art, solid-state high voltage modulator. We have chosen the solid-state modulator (K2-3X) built by ScandiNova for its pulse-to-pulse stability and solid-state modular design; the first of these modulators has been delivered and is awaiting installation. Two klystrons and two high voltage modulators are planned for the LLNL MEGa-Ray project.

The high power pulsed RF output of two klystrons is 100 MW, 1.5 msec. The high power RF needs of the RF gun and accelerator sections are 440 MW for 210 ns (~3x fill time). The logical way to achieve this is to pulse compress the output of the klystrons to 500 MW, 210 ns and to distribute the compressed pulse to the RF gun and accelerating sections. SLAC has developed and demonstrated SLED II with multi-mode delayed lines with similar power gain factor [12]. The dual-mode SLED-II delay lines will be approximately 15 meter long with inner diameter of 17 cm.

500 MW, 210 ns pulses are the desired output of the pulse compression system. These compressed pulses will be fed into a 13 dB coupler. The 13 dB (25 MW) output will go to the RF gun. To allow for tuning and control, a phase shifter and attenuator are put in this arm. A barrier window is also planned for the RF gun. This is to limit the number of times the RF gun is exposed to air and to possibly provide for a configuration in which the RF gun can be baked and sealed as a unit before installation. The rest of the compressed power (475 MW) is to be distributed to the linear accelerator sections. A 3 dB H-hybrid is used to divide the 475 MW in half. Then a combination and 4.8 dB and 3 dB H-hybrids are used to distribute the power in one-third portion (~70 MW) to each T53 section. Phase shifters and other control elements will be added as needed.

## SYNCHRONIZATION

To ensure synchronization between the electron-generating laser pulse, the scattering laser pulse, and the electron-accelerating RF power, the fiber-based laser oscillator is used as a universal clock. The oscillator runs at a sub-harmonic of the RF design frequency (40.8 MHz for a 11.424 GHz accelerator), and provides seed light to both amplifier systems. The oscillator pulse train is monitored by a high-speed photodiode and the 11.424 GHz component of the signal is selected by a narrow band-pass filter, amplified, and delivered to the RF power system. Because the laser pulses start from the same oscillator, they are guaranteed to have good relative stability – all that is required it to match the travel time to the interaction point. Selecting correct pulses from the oscillator will get the pulses within 24 ns, and an extra length of optical fiber in the pre-amplification system can get to ~ns resolution. Final ps accuracy comes from an optical delay arm with micron accuracy.

## PHOTOCATHODE DRIVE LASER

The photo-electrons are generated by a 50 μJ, 263 nm spatially and temporally shaped laser pulse. The oscillator seed is amplified (using standard CPA methods) in a series of Yb-doped fiber amplifiers, beginning with standard 6-μm core pre-amps, a 29 μm core intermediate photonic crystal fiber stage and a final 85 μm fiber rod amplifier to generate 1 mJ, 1053 nm pulses at 120 Hz that are compressed to 250 fs. These pulses are frequency quadrupled, stacked in a "Hyper-Michelson" pulse stacker, which converts the single input pulse into 8 replicas using 3 beam splitters; then transformed from Gaussian to a flat-top transverse profile using refractive optical beam shaping components. This beam is transported to the photoinjector, resized to 1 mm, and imaged onto the cathode surface.


[1] M. Y. Shverdin, *et al*., Opt. Lett. **35**, 14 (2010).
[2] F. Albert, *et al*., Opt. Lett. **35**, 354 (2010).
[3] D.J. Gibson, *et al*., Phys. Rev. STAB **13**, 070703 (2010).
[4] F. Albert, *et al*., Phys. Rev. STAB **13**, 070704 (2010).
[5] L.M. Brown and R.P. Feynman, Phys. Rev. **85**, 231 (1952).
[6] G. Bhatt, *et al*., Phys. Rev. A **28**, 2195 (1983).
[7] F.V. Hartemann, *et al*., Phys. Rev. Lett. **105**, 130801 (2010).
[8] I.V. Bazarof, *et al*., Phys. Rev. Lett. **102**, 104801 (2009).
[9] Y. Ding, *et al*., Phys. Rev. Lett. PRL **102**, 254801 (2009).
[10] D.J. Gibson, *et al*., Phys. Rev. STAB **4**, 090101 (2001)
[11] A.E. Vlieks, *et al*., SLAC-PUB-11689 (2006); AIP Conf. Proc. **807**, 481 (2006).
[12] S. G. Tantawi, *et al*., Phys. Rev. STAB **8**, 042002 (2005).